On the Spectral Similarity of Bridging and Nonbridging Oxygen in Tellurites

R. T. Hart,[†] J. W. Zwanziger,*[,‡] U. Werner-Zwanziger,[‡] and J. R. Yates[§]

Intense Pulsed Neutron Source, Argonne National Laboratory, Argonne, Illinois, Department of Chemistry and Institute for Research in Materials, Dalhousie University, Halifax, NS, Canada, and Cavendish Laboratory, University of Cambridge, Cambridge, U.K.

Received: May 9, 2005; In Final Form: June 24, 2005

We show by high field ^{17}O solid-state nuclear magnetic resonance (NMR) and by ab initio calculations of both the NMR and the oxygen 1s photoelectron spectra that the oxygen sites in tellurite glasses show no spectroscopic distinction, even when comparing bridging and nonbridging sites. This is remarkable because two such sites differ formally by a full electronic charge, and they are readily distinguished by these same methods in silicates. We argue that this similarity arises from the symmetry breaking that occurs when the original TeO_2 crystal solid forms, due to the pseudo-Jahn−Teller distortion induced by the two additional valence electrons present in Te^{IV} as compared to Si^{IV}.

1. Introduction

Simple oxide glasses, especially silicates, contain two characteristic oxygen bonding geometries: bridging oxygen (BO), in which the oxygen is covalently bonded to two main group atoms, and nonbridging oxygen (NBO), in which the oxygen is bonded to a single main group atom and participates in ionic interactions with modifiers. An example of BO would be −Si−O−Si−, while a typical NBO is $-Si-O^-Na^+$. Such modification is of great importance in glass technology, as a route to control the thermal and mechanical properties of the resultant glass. Since modification results in the replacement of strong covalent bonds with weaker ionic interactions, the softening point, glass transition temperature, and so forth can be greatly reduced.

Because of the formal charge difference between bridging and nonbridging oxygen, these two species are usually easy to distinguish by a number of different methods, including X-ray photoelectron spectroscopy (XPS) and nuclear magnetic resonance spectroscopy (NMR).[1−3] Furthermore, the bond length difference between BO and NBO (about 1.65 vs 1.59 Å in silicates) makes them resolvable by neutron diffraction.[4]

Telluria (TeO_2) also gives rise to oxide solids, but the bonding geometries are more complex than in the silicates.[5,6] In particular, in tellurite crystals nonbridging oxygen with a single formal negative charge are not usually observed; instead, two nonbridging oxygens sharing a single negative charge, or three nonbridging oxygens sharing two negative charges, are frequently seen.[7] Nevertheless, as in the silicates these structures do result from addition of an alkali oxide like Na_2O, with the concomitant cleavage of covalent Te−O bonds, so that telluria is modifiable in much the same way as silica. The mechanical consequences, such as significant lowering of the glass transiiton temperature, are similar to those seen in silicates.[8] The bridging and nonbridging oxygen bond lengths are resolved by neutron diffraction,[5,6] but unlike the silicates, the BO's and NBO's are not resolved in XPS.[1,9] As in the case of silicates, one would expect that ^{17}O solid-state NMR should also show resolution of the BO and NBO in tellurites, and indeed we found previously that in crystalline TeO_2 and Na_2TeO_3, the oxygens have rather different NMR parameters.[10] These cases are extreme, however, in that TeO_2 has only bridging oxygen,[11] while Na_2TeO_3 is an ionic solid consisting of isolated TeO_3^{2-} anions coordinated by Na^+.[12]

We show in this paper that even at a relatively high field (16.44 T), the oxygen sites in glassy sodium tellurites are not resolved. This negative result is interesting in that it demonstrates along with the XPS data that the BO and NBO in tellurites are remarkably similar in electronic structure. We then provide detailed ab initio calculations of both the XPS data and the NMR data, to derive an understanding of the origin of this similarity. Finally, we contrast this system to the better-known silicate case.

2. Methods

2.1. Experimental Methods. 2.1.1. Sample Preparation. ^{17}O-enriched α-tellurite (α-$Te^{17}O_2$) was synthesized from tellurium isopropoxide (85%, Alfa Aesar) and water (99.9999%, 40% ^{17}O, Cambridge Isotope Labs).[10] When 2 equiv of water were added to a stirring ethanol solution of $Te(OiPr)_4$, $Te^{17}O_2$ was obtained instantly as a white precipitate. The reaction was followed by recrystallization in air, accomplished by melting the resulting white powder at 750 °C in a nonwetting ZGS Pt/Au crucible and cooling at 2 °C/min. As TeO_2 has very low volatility at this temperature, no loss in enrichment was observed due to the recrystallization step. After recrystallization, α-$Te^{17}O_2$ was obtained quantitatively as off-white needles. The phase purity was confirmed by solid state ^{125}Te MAS NMR, powder X-ray diffraction, and Raman spectroscopy.

Glasses were prepared by melting α-$Te^{17}O_2$ together with Na_2CO_3 in a Pt crucible at 800 °C for 10 min and quenching in ice−water. The resulting materials were amorphous by X-ray diffraction and showed glass transition temperatures by differential scanning calorimetry in accordance with literature values.[8]

* To whom correspondence should be addressed. E-mail: jzwanzig@dal.ca.
[†] Argonne National Laboratory.
[‡] Dalhousie University.
[§] University of Cambridge.

10.1021/jp052405h CCC: $30.25
Published on Web 07/28/2005

2.1.2. NMR Spectroscopy. Spectra at 9.4 T (54.5 MHz ^{17}O resonance frequency were acquired on a Bruker DSX spectrometer, under magic angle spinning conditions (12.0 kHz). A Hahn echo sequence was used, with 4 and 8 μs times for the 90 and 180° pulses, respectively. A 500 s recycle delay was used, and each spectrum consists of 2048 scans.

^{17}O NMR spectra at 16.4 T (^{17}O Larmor frequency of 94.9 MHz) were acquired on a Bruker Avance NMR spectrometer, using 2.5 mm rotors and magic angle spinning at 30.0 kHz. We employed a 2-dimensional multiple rotor-assisted population transfer (RAPT) pulse sequence with Hahn echo detection.[13] The RAPT transfer was repeated 21 times followed by acquisition of the free induction decay. 64 blocks of these spectra were acquired in rapid succession and saved as a 2-dimensional data set. A total of 724 scans (10% and 30% Na2O) or 1272 scans (20% Na2O), respectively, were accumulated with a repetition delay of 350 s. The spectra shown below are center slices after Fourier transformation in both dimensions.

2.2. Computational Methods. 2.2.1. Molecular Modeling. Modeling of molecular TeF_4 and SiF_4 was carried out with the Amsterdam density functional code (ADF).[14−16] Because the object of this part of the study was only to develop a qualitative Walsh diagram relating molecular shape to orbital energies, a small basis set, double-ζ STO, was used, together with frozen core orbitals. Generalized gradient corrections to the local density approximation as proposed by Becke,[17] for exchange, and Perdew,[18] for correlation, were employed.

2.2.2. Modeling Solids, XPS Data, and NMR Spectra. Results relating to simulation of the XPS data were obtained through use of the ABINIT code, which is based on pseudopotentials and planewaves.[19] This is a density functional theory approach to finding the energies of periodic solids, in which the valence electron wave functions are expanded in terms of planewaves, and the effect of the core electrons are approximated through the use of pseudopotentials. Pseudopotentials were generated with the FHI98PP code.[20] For the cases discussed below, the pseudopotentials used were of Troullier−Martins type,[21] in separable form. For all atomic species studied (Te, O, Na, Si), we used a maximum angular momentum value of 2 for generation of the pseudopotentials, and also $l = 2$ for the local potential. For all elements, only the outer s and p electrons were treated as valence electrons; in addition, for Na, nonlinear core corrections[22] were used to account for the core−valence overlap from the relatively diffuse 2p orbitals.

For both the pseudopotentials and the calculations on the periodic solids, the generalized gradient approximation for the exchange and correlation terms due to Perdew, Burke, and Enzerhof was used.[23] For oxygen, an additional pseudopotential with valence configuration $1s2s^22p^5$ was generated, for use in simulating oxygen 1s XPS data. All pseudopotentials constructed were checked for existence of "ghost" states[24] through the tests available in the FHI98PP package and examination of the logarithmic derivatives. Transferability tests were performed by checking that the eigenvalues of the pseudoatoms and the all-electron atoms agreed for a variety of test configurations, in which partial charges were transferred from lower lying to higher lying valence states or ionized completely.

As discussed below, the ab initio computations used here are of the total energy of the model crystals, with defects at different locations. In all cases, a planewave cutoff energy of 30 Ha (816 eV) was used. The necessary integration over reciprocal space was performed by using an optimum grid, in the sense of fewest *k*-points, for which the shortest vector in real space not included was about 18.5 Å (this corresponded to a spacing in reciprocal space of about 0.05 $Å^{-1}$). For $Na_2Si_2O_5$ this approach amounted to a $4 \times 2 \times 4$ Monkhorst-Pack grid, and for $Na_2Te_4O_9$, a $3 \times 2 \times 3$ Monkhorst-Pack grid.[25] The other samples have more complex primitive unit cells and so have more complex descriptions. All grids used were offset from the origin by 0.5 units in reciprocal space. Such optimal grids are computed by the ABINIT code. The energies were computed using the experimentally determined crystal structures.

XPS results were modeled using a thermodynamic cycle approach.[26,27] In this approach, it is noted first that extraction of a core electron results in a solid with a core-ionized atom at a specific site. The energy required to extract the electron is the quantity observed in the XPS measurement. On the other hand, the cohesive energy of the resulting defective solid relative to free atoms can be computed by the planewave pseudopotential method. This is done by representing the defective atom with a pseudopotential constructed from an atom with a core hole. In a second calculation, the defect is placed at a chemically distinct site. The free atom reference state is the same in both cases. Furthermore, in both cases the original, defect-free solid as probed by XPS is the same. Therefore, one has

$$E_B + E_C = E'_B + E'_C \tag{1}$$

where E_B is the binding energy of the core electron at the first site and E_C the cohesive energy of the resulting defective solid, and the primed quantities refer to the defect appearing at the second site. The shift between the binding energies can then be computed as

$$E_B - E'_B = -(E_C - E'_C) \tag{2}$$

Thus, the chemical shifts of an XPS spectrum can be computed, despite the fact that the absolute values of the binding energies cannot.

Replacing normal oxygen by a core hole oxygen lowers the symmetry of the crystal, and this is taken into account in constructing the *k*-space grid by ABINIT. Moreover, the interactions between defects (in neighboring unit cells) should be considered. We found however that for the relatively large unit cells studied here, and at the 0.5 eV resolution necessary for distinguishing different XPS shifts, replacing the unit cell by a larger supercell made no significant difference in the energy shifts.

The NMR parameters were computed using the NMR module[28,29] of the CASTEP code.[30] This code also uses a density functional theory approach within the planewave/pseudopotential formalism. Additionally it includes code to calculate the magnetic field response and the electric field gradient tensors. This method has been validated recently on a variety of oxide and glassy materials.[31] The calculations were performed using Troullier−Martins[21] pseudopotentials. Pseudopotentials for Na and O were generated using parameters given in ref 31 and for Te using parameters given in ref 32. All calculations used the experimental crystal structures. The PBE[23] exchange-correlation functional was used and the wave functions expanded in planewaves with a maximum energy of 50 Ha.

The output of an ab initio NMR calculation is the absolute chemical shielding tensor, $\bar{\sigma}_{iso}(r)$ defined as the ratio between a uniform external magnetic field, *B*, and the induced magnetic field $B_{in}(r)$

$$B_{in}(r) = -\bar{\sigma}_{iso}(r)B \tag{3}$$

The isotropic shielding $\sigma_{iso}(r)$, is one-third of the trace of

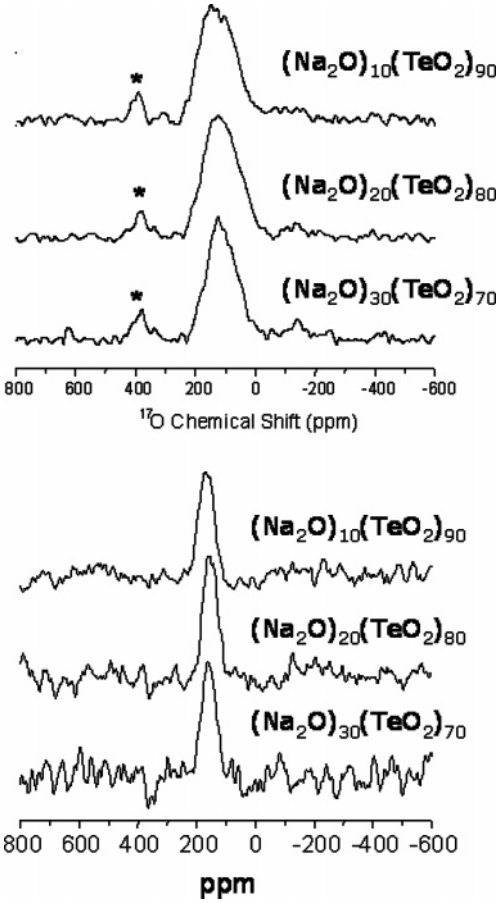

Figure 1. ^{17}O magic angle spinning NMR spectra of sodium tellurite glasses, of the stated compositions. Top: 9.4 T field (54 MHz oxygen resonance), Hahn echo sequence. Asterisks denote spinning sidebands. Bottom: 16.4 T field (94.9 MHz oxygen resonance, multiple RAPT sequence).

$\bar{\sigma}_{iso}(r)$. To compare directly with experimentally measured isotropic chemical shifts we use

$$\delta_{iso}(r) = -[\sigma_{iso}(r) - \sigma_{ref}] \quad (4)$$

with $\sigma_{ref} = 259.32$ ppm taken from previous work on glassy materials.[31]

The quadrupolar coupling constant, C_Q and the asymmetry parameter, η values were extracted from the diagonalized electric field gradient tensor whose eigenvalues are labeled V_{xx}, V_{yy}, and V_{zz}, such that $|V_{zz}| > |V_{yy}| > |V_{xx}|$:

$$C_Q = eV_{zz}Q_0/h \quad (5)$$

where h is Planck's constant and

$$\eta_Q = (V_{xx} - V_{yy})/V_{zz} \quad (6)$$

We use a value for the electric quadrupole moment of the oxygen nucleus of $Q_O = 2.55$ fm^2.[31]

3. Results

^{17}O NMR spectra of the tellurite glasses are shown in Figure 1 for two fields, 9.4 and 16.44 T (^{17}O frequencies of 54 and 95 MHz, respectively). Table 1 and Figure 2 show results of the simulated oxygen 1s XPS shifts, for several model crystals: Na_2SiO_3, $Na_2Si_2O_5$, $Na_2Te_4O_9$, and $Na_2Te_2O_5$. In each case, the shifts are referenced to the average of the bridging oxygen shifts.

Table 2 shows computational and experimental results for the ^{17}O NMR parameters in tellurite crystals, including α-TeO_2, $Na_2Te_4O_9$, $Na_2Te_2O_5$, and Na_2TeO_3. These systems differ significantly in the range and types of bridging and nonbridging oxygen they have.

TABLE 1: Computed Oxygen 1s XPS Shifts for Sites in Crystalline Na_2SiO_3, $Na_2Si_2O_5$, $Na_2Te_4O_9$, and $Na_2Te_2O_5$, together with Hirshfeld Net Charge Analysis for Each, in Units of the Magnitude of the Electron Charge[a]

crystal	site	shift/eV	net charge/|e$^-$|
Na_2SiO_3	BO-1	0.00	−0.22
	NBO-1	−1.69	−0.37
$Na_2Si_2O_5$	BO-1	0.09	−0.22
	BO-2	−0.09	−0.23
	NBO-1	−1.71	−0.39
$Na_2Te_4O_9$	BO-1	0.11	−0.28
	BO-3	0.05	−0.27
	BO-5	0.19	−0.27
	BO-6	−0.30	−0.25
	BO-7	0.08	−0.28
	BO-8	−0.10	−0.31
	BO-9	−0.03	−0.25
	NBO-2	−0.41	−0.29
	NBO-4	0.18	−0.32
$Na_2Te_2O_5$	BO-4	−0.18	−0.26
	BO-5	0.18	−0.27
	NBO-1	−0.56	−0.33
	NBO-2	−0.24	−0.32
	NBO-3	−0.22	−0.30

[a] BO and NBO refer to bridging oxygen and nonbridging oxygen, respectively. The shifts are referenced to the average of the BO shifts in each case.

TABLE 2: Theoretical and Experimental[10] Results for ^{17}O NMR Parameters in Crystalline Tellurites

		theory			experiment		
site	type	C_Q (MHz)	η_Q	δ_{iso} (ppm)	C_Q (MHz)	η_Q	δ_{iso} (ppm)
				TeO_2			
O-1	BO	7.78	0.48	199.53	7.48	0.43	180
				$Na_2Te_4O_9$			
O-1	NBO	6.74	0.56	251.81			
O-2	BO	6.55	0.47	241.37			
O-3	BO	6.21	0.43	233.26			
O-4	NBO	7.20	0.17	218.31			
O-5	BO	6.12	0.88	254.80			
O-6	BO	7.14	0.46	232.07			
O-7	BO	6.82	0.53	226.46			
O-8	NBO	7.45	0.21	187.32			
O-9	BO	7.14	0.71	219.20			
				$Na_2Te_2O_5$			
O-1	BO	7.65	0.25	230.04			
O-2	NBO	7.05	0.04	207.21			
O-3	NBO	6.53	0.27	255.58			
O-4	BO	5.91	0.57	220.03			
O-5	BO	6.41	0.49	279.19			
				Na_2TeO_3			
O-1	NBO	6.16	0.12	182.3	6.63	0.33	158
O-2	NBO	6.28	0.10	171.01			
O-3	NBO	6.41	0.02	214.61			

4. Discussion

4.1. Bonding in Tellurium-Centered Molecules. Understanding the bond lengths in tellurites is critical to understanding their response to modification, and tellurium-centered molecules are the simplest starting point.

Figure 3 shows a simple molecular orbital diagram for SiF_4, in its experimental ground-state geometry, as derived from ab initio calculations. Note that no antibonding orbitals are occupied. Orbitals $2a_1$ and $2t_2$ together make up the σ-bonding

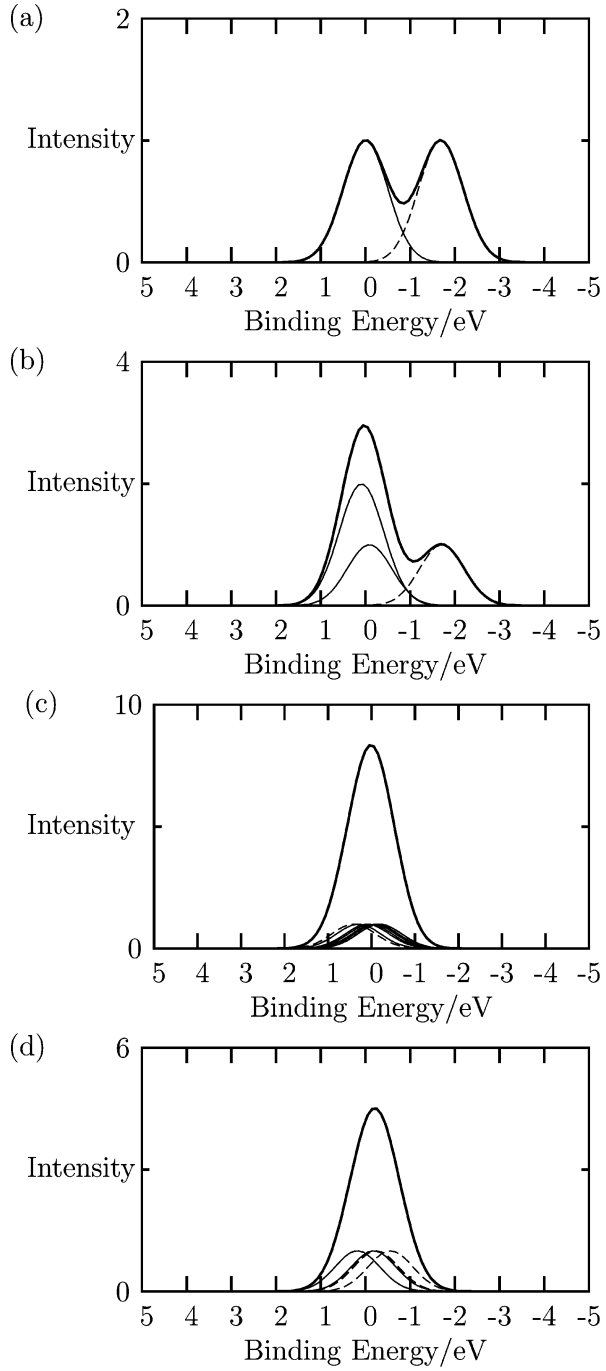

Figure 2. Model oxygen 1s XPS spectra computed for (a) Na_2SiO_3, (b) $Na_2Si_2O_5$, (c) $Na_2Te_4O_9$, and (d) $Na_2Te_2O_5$. Spectra computed from ab initio calculations as outlined in the text, using a pseudopotential with a 1s hole. Spectra have been artificially broadened with Gaussians of width 0.5 eV. In each plot, bridging oxygen sites are plotted with solid lines, nonbridging oxygen sites with dashed lines, and the total sum with heavy solid lines.

orbitals, which in the nomenclature of hybridization gives rise to sp^3 bonding. The electrons in orbitals 1e, $1t_1$, and $3t_2$ arising from the fluorine atoms are nonbonding lone pairs. The change from SiF_4 to TeF_4 in this geometry leads to addition of the two circled electrons into the $3a_1^*$ antibonding orbital. This addition is not sufficient to destabilize the molecule relative to neutral atoms, but does nevertheless lead to a symmetry-breaking distortion to a C_{2v} structure. This distortion can be understood as arising from a pseudo-Jahn−Teller mechanism, in which the occupied $3a_1^*$ orbital interacts through the shape distortion with the lowest unoccupied orbital, here of symmetry t_2, to produce

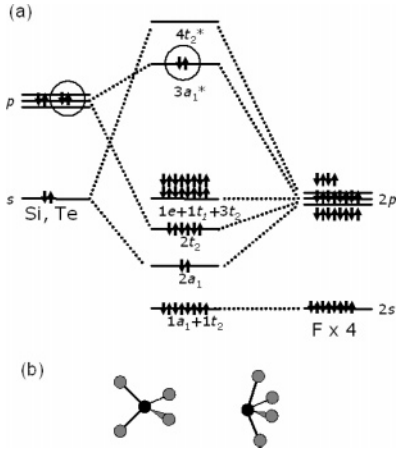

Figure 3. (a) Simple molecular orbital energy level scheme for SiF_4 and TeF_4 in tetrahedral geometry. The difference between the two arises from the addition pair of electrons from Te (circled), which would occupy an antibonding orbital. The distortion this causes is depicted in part b, where the tetrahedral shape (left) is contrasted with the C_{2v} distortion adopted by TeF_4.

a lower energy, lower symmetry structure.[33] One might guess that the resulting shape (four bonds in a C_{2v} geometry plus a lone pair) would require the use of d-orbitals on the tellurium, but it is well-established that main group molecules such as this do not use d-orbitals to form hybridized sets for bonding.[34,35] The bond that forms in addition to the original directed σ bonds, is best described as a three-center, four-electron bond across the two axial fluorine and the tellurium atom. This weak bond retains antibonding character, and it is doubtless why these bonds are longer than the bonds to the equatorial fluorine ligands.

This bonding pattern persists into the solid state, with an interesting alternating pattern.[11] The crystal structure of TeO_2 shows it to consist of TeO_4 polyhedrons, with shapes very similar to molecular TeF_4, including local C_{2v} symmetry, two long axial bonds, and two short equatorial bonds. In addition, the oxygens in the axial positions are bonded equatorially to adjacent Te atoms, and the equatorial oxygens are bonded axially to adjacent Te atoms. In other words, each oxygen participates in TeO_2 in both a long and a short bond, in contrast to the oxygen in SiO_2, in which all Si−O bonds are equivalent.

4.2. XPS and NMR Data: Comparison with Theory. Since the short-range structures of amorphous and crystalline oxides are similar,[36] crystalline model compounds were used for calculation of the XPS shifts. These included $Na_2Te_4O_9$, $Na_2Te_2O_5$, $Na_2Si_2O_5$, and Na_2SiO_3. All four of these compounds include a mix of bridging and nonbridging oxygens. Na_2SiO_3 includes two equivalent bridging and two equivalent nonbridging oxygens on each silicon.[37] $Na_2Si_2O_5$ has two types of bridging oxygens and one type of nonbridging oxygen, in a 2:1:2 ratio.[38] $Na_2Te_4O_9$ has nine distinct oxygen sites, six or seven of which are bridging (depending on what cutoff criterion is used).[39] Finally, $Na_2Te_2O_5$ has five distinct oxygen sites, two of which are bridging.[40]

We computed the oxygen 1s XPS chemical shift between the different sites in these crystals, following the methodology outlined in eq 2 above, and the results are summarized in Figure 2 and Table 1. Table 1 shows that there is a significant shift (about 1.7 eV) between the bridging and nonbridging sites in the silicates, just as is observed in experiments[1] while in the tellurites there is almost no discernible correlation between shift and site. Figure 2 shows in fact that the tellurite shifts lie virtually on top of one another, leading to a total lack of

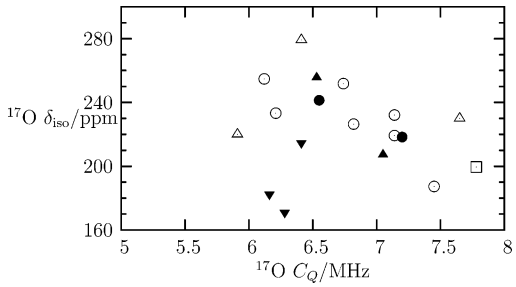

Figure 4. Correlation between calculated isotropic chemical shift and quadrupole coupling strength for ^{17}O in tellurite crystals (data plotted from Table 2). In all cases open symbols represent bridging oxygen, and filled symbols represent nonbridging oxygen. Squares: TeO_2. Circles: $Na_2Te_4O_9$. Triangles (point up): $Na_2Te_2O_5$. Triangles (point down): Na_2TeO_3.

resolution of the bridging and nonbridging sites. To be sure, in the $Na_2Te_2O_5$ sample the nonbridging oxygen shifts are all at slightly lower binding energies than the bridging sites, so it would appear that as the ionic environment in tellurites increases, the bonding follows increasing silicate-like patterns.

The difference between the two types of sites was examined more quantitatively by using Hirshfeld charge analysis[41] to assess the electron density around each oxygen. In the silicate we found that the nonbridging oxygen holds about 0.17−0.19 e^- more net charge than the bridging site, while in the tellurite the total spread over all sites, from most charged to least, is only 0.07 e^-. Again, there is no noticeable correlation between the charge and the structural nature of the site. We note also that the magnitudes of the charges on the oxygen in the silicates span that in the tellurites, such that the silicate BO sites have less charge, and the NBO sites have more charge, than the tellurite sites, with the tellurite charge values falling roughly in the middle. Hirshfeld charge analysis on SiO_2 and TeO_2 give respectively $-0.22|e^-|$ and $-0.27|e^-|$ as the net charges on oxygen, both of which agree well the values computed for the bridging sites in the silicates and tellurites.

Like oxygen 1s XPS, ^{17}O NMR typically shows a significant distinction between bridging and nonbridging sites in oxide glasses. However, we found that even at moderately high field (16.44 T, 95 MHz oxygen resonance frequency) the Magic Angle Spinning spectra do not show any clear indication of multiple sites with differing shifts or quadrupole coupling constants (Figure 1). In contrast, at this field strength a silicate glass such as $Na_2Si_2O_5$ would show clear resolution of the bridging and nonbridging sites (based on published values of the oxygen NMR parameters[3]). The observed resonances do narrow on going from the lower to the higher field, by a factor of roughly two in ppm units. In this case the field has increased by a factor of 16.44/9.4, or 1.74; since second order quadrupole broadening varies as the inverse field squared, again when using ppm units for the shift, we would anticipate a narrowing by a factor of about 3. The remaining width is presumably due to the intrinsic disorder, since even at extremely high magnetic fields a glass would not give sharp NMR resonances. However, no hint of resolution of two oxygen environments is apparent.

The ab initio calculations of the ^{17}O NMR parameters show a similar overlap between the different types of sites in crystalline tellurites (Table 2). Figure 4 shows the very minimal correlation that exists between the isotropic chemical shift and the quadrupole coupling strength for ^{17}O in the various tellurite crystals; one sees that there is no clear separation between the two types of sites plotted in this way. This is in contrast to silicates, for which it has been shown previously that this type of plot gives a very clear distinction between bridging and nonbridging sites.[31] The lack of correlation in Figure 4 thus provides further evidence that in the tellurites these sites have quite similar electronic structure.

4.3. Origin of Differences to Silicates. It is apparent, based on the XPS and NMR data and the ab initio calculations, that bridging and nonbridging oxygens in tellurites have electronic environments that are remarkably similar, in sharp contrast to what is observed in silicates. We now suggest a reason for this similarity. We noted in Figure 3 that the energetic cost of the extra pair of antibonding electrons in a molecule like TeF_4, as compared to SiF_4, is at least partially regained by distorting to a lower symmetry structure. In this new structure, there are both long bonds and short bonds, the long bonds including the majority of the antibonding character of the additional pair of electrons. When these units are linked in α-TeO_2, each oxygen participates in both a long and a short bond, connected to neighboring tellurite atoms. In silica, by contrast, all Si−O bonds are equivalent. Therefore, it appears that in telluria *already for bridging oxygen* there is a broken symmetry. When the material is modified by adding an alkali oxide, such as Na_2O, and bonds break to accommodate the additional charge of the sodium cations and the additional oxygen atoms, it is reasonable to assume that the longer (weaker) of the two bonds will break preferentially. Then when we compare the spectral response of these newly formed nonbridging oxygen with the response of the bridging conformation, we must remember that we are comparing an oxygen with a short Te−O bond to one that did have two bonds but for which one was extended and had more antibonding character. Morever, as we saw from Hirshfeld charge analysis, the additional charge introduced into the oxide network through alkali ion modification is spread more evenly over the oxygen sites in the tellurites, presumably facilitated by the three-center four-electron bond. Thus, in the final analysis, it is perhaps not so surprising that the bridging and nonbridging oxygen sites appear similar spectroscopically in the tellurites; the distinction between bridging and nonbridging has already been mostly lost in the unmodified starting material, TeO_2.

5. Conclusions

We have shown in this paper that both the oxygen 1s XPS and ^{17}O NMR spectra of tellurites do not resolve the distinction between bridging and nonbridging oxygen. These structures are clearly resolved in silicates, and they play a large role in understanding the mechanical and thermal properties of glasses. We showed also that high level ab initio calculations indicate for both XPS and NMR that the bridging and nonbridging sites respond in a very similar way. We conclude from this study that the reason for this similarity lies in the broken symmetry inherent in the original α-TeO_2 structure, for which the additional antibonding electrons of TeX_4, as compared to SiX_4, induce an asymmetry between Te−X bonds. Both long (weaker) and short (stronger) bonds are already present in α−TeO_2; upon modification, this dissimilarity of course persists, but upon comparing the spectral responses of the two cases, there is relatively little change.

Acknowledgment. J.W.Z. thanks Prof. Neil Burford and Prof. Russ Boyd for many helpful conversations. Financial support for this research came from the US National Science Foundation, the Canada Foundation for Innovation, the Canada Research Chairs program, and the Natural Sciences and Engineering Research Council of Canada.

References and Notes

(1) Himei, Y.; Miura, Y.; Nanba, T.; Osaka, A. *J. Non-Cryst. Solids* **1997**, *211*, 64−71.
(2) Florian, P.; Vermillion, K. E.; Grandinetti, P. J.; Farnan, I.; Stebbins, J. F. *J. Am. Chem. Soc.* **1996**, *118*, 3493−3497.
(3) Maekawa, H.; Florian, P.; Massiot, D.; Kiyono, H.; Nakamura, M. *J. Phys. Chem.* **1996**, *100*, 5525−5532.
(4) Du, J.; Cormack, A. N. *J. Non-Cryst. Solids* **2004**, *349*, 66−79.
(5) McLaughlin, J. C.; Tagg, S. L.; Zwanziger, J. W. *J. Phys. Chem. B* **2001**, *105*, 67−75.
(6) Niida, H.; Uchino, T.; Jin, J. S.; Kim, S. H.; Fukunaga, T.; Yoko, T. *J. Chem. Phys.* **2001**, *114*, 459−467.
(7) Becker, C. R.; Tagg, S. L.; Huffman, J. C.; Zwanziger, J. W. *Inorg. Chem.* **1997**, *36*, 5559−5564.
(8) Heo, J.; Lam, D.; Sigel, G. H., Jr.; Mendoza, E. A.; Hensley, D. A. *J. Am. Ceram. Soc.* **1992**, *75*, 277−281.
(9) Lim, J. W.; Jain, H.; Toulouse, J.; Marjanovic, S.; Sanghera, J. S.; Miklos, R.; Aggarwal, I. D. *J. Non-Cryst. Solids* **2004**, *349*, 60−65.
(10) Hart, R. T., Jr.; Zwanziger, J. W. *J. Am. Ceram. Soc.* **2005**, in press.
(11) Lindqvist, O. *Acta Chem. Scand.* **1968**, *22*, 977−982.
(12) Masse, R.; Guitel, J. C.; Tordjman, I. *Mater. Res. Bull.* **1980**, *15*, 431−436.
(13) Kwak, H.-T.; Prasad, S.; Clark, T.; Grandinetti, P. J. *Solid State NMR* **2003**, *24*, 71−77.
(14) te Velde, G.; Bickelhaupt, F. M.; van Gisbergen, S. J. A.; Foncesca Guerra, C.; Baerends, E. J.; Snijders, J. G.; Ziegler, T. *J. Comput. Chem.* **2001**, *22*, 931−967.
(15) Foncesca Guerra, C.; Snijders, J. G.; te Velde, G.; Baerends, E. J. *Theor. Chem. Acc.* **1998**, *99*, 391−403.
(16) "ADF2002.03", http://www.scm.com. Theoretical Chemistry, Vrije Universiteit: Amsterdam, The Netherlands.
(17) Becke, A. D. *Phys. Rev. A* **1988**, *38*, 3098−3100.
(18) Perdew, J. P. *Phys. Rev. B* **1986**, *33*, 8822.
(19) Gonze, X.; et al. *Comput. Mater. Sci.* **2002**, *25*, 478−492.
(20) Fuchs, M.; Scheffler, M. *Comput. Phys. Commun.* **1999**, *119*, 67.
(21) Troullier, N.; Martins, J. L. *Phys. Rev. B* **1991**, *43*, 1993−2006.
(22) Louie, S. G.; Froyen, S.; Cohen, M. L. *Phys. Rev. B* **1982**, *26*, 1738−1742.
(23) Perdew, J. P.; Burke, K.; Ernzerhof, M. *Phys. Rev. Lett.* **1996**, *77*, 3865−3868.
(24) Gonze, X.; Stumpf, R.; Scheffler, M. *Phys. Rev. B* **1991**, *44*, 8503−8513.
(25) Monkhorst, H. J.; Pack, J. D. *Phys. Rev. B* **1976**, *13*, 5188−5192.
(26) Johansson, B.; Mårtensson, N. *Phys. Rev. B* **1980**, *21*, 4427−4457.
(27) Mäder, K. A.; Baroni, S. *Phys. Rev. B* **1997**, *55*, 9649−9658.
(28) Pickard, C. J.; Mauri, F. *Phys. Rev. B* **2001**, *63*, DOI 245101.
(29) Profeta, M.; Mauri, F.; Pickard, C. J. *J. Am. Chem. Soc.* **2003**, *125*, 541.
(30) Segall, M. D.; Lindan, P. J. D.; Probert, M. J.; Pickard, C. J.; Hasnip, P. J.; Clark, S. J.; Payne, M. C. *J. Phys.: Cond. Matt.* **2002**, *14*, 2717−2743.
(31) Charpentier, T.; Ispas, S.; Profeta, M.; Mauri, F.; Pickard, C. *J. Phys. Chem. B* **2004**, *108*, 4147−4161.
(32) Yates, J.; Pickard, C.; Mauri, F.; Payne, M. *J. Chem. Phys.* **2003**, *118*, 5746−5753.
(33) Atanasov, M.; Reinen, D. *Inorg. Chem.* **2004**, *43*, 1998−2012.
(34) Kutzelnigg, W. *Angew. Chem., Int. Ed. Engl.* **1984**, *23*, 272−295.
(35) Reed, A. E.; Weinhold, F. *J. Am. Chem. Soc.* **1986**, *108*, 3586−3593.
(36) Zwanziger, J. W. *Int. Rev. Phys. Chem.* **1998**, *17*, 65−90.
(37) McDonald, W. S.; Cruickshank, D. W. J. *Acta Crystallogr.* **1967**, *22*, 37−43.
(38) Pant, A. K. *Acta Crystallogr. B* **1968**, *24*, 1077−1083.
(39) Tagg, S. L.; Huffman, J. C.; Zwanziger, J. W. *Chem. Mater.* **1994**, *6*, 1884−1889.
(40) Tagg, S. L.; Huffman, J. C.; Zwanziger, J. W. *Acta Chem. Scand.* **1997**, *51*, 118.
(41) Hirshfeld, F. L. *Theor. Chim. Acta* **1977**, *44*, 29.